Electronic Supplementary Material (ESI) for Journal of Materials Chemistry A.
This journal is © The Royal Society of Chemistry 2019

Electronic Supplementary Information

Janus Membranes with Controllable Asymmetric Configuration for Highly Efficient Separation of Oil-in-Water Emulsions

Jing Yang†, Hao-Nan Li†, Zhi-Xiong Chen, Ai He, Qi-Zhi Zhong, Zhi-Kang Xu*

MOE Key Laboratory of Macromolecular Synthesis and Functionalization, and Key Laboratory of Adsorption and Separation Materials & Technologies of Zhejiang Province, Department of Polymer Science and Engineering, Zhejiang University, Hangzhou 310027, China

*E-mail: xuzk@zju.edu.cn

†These authors contributed equally to this work

Table of Contents

Figure S1 – Figure S2----------S3

Figure S3 – Figure S4----------S4

Figure S5----------S5

Table S1----------S6

Figure S6 – Figure S7----------S7

Figure S8 – Figure S9----------S8

Figure 10 and Table S2----------S9

Figure S11 ----------S10

Figure S12 – Figure S13----------S11

Figure S14----------S12

References----------S12

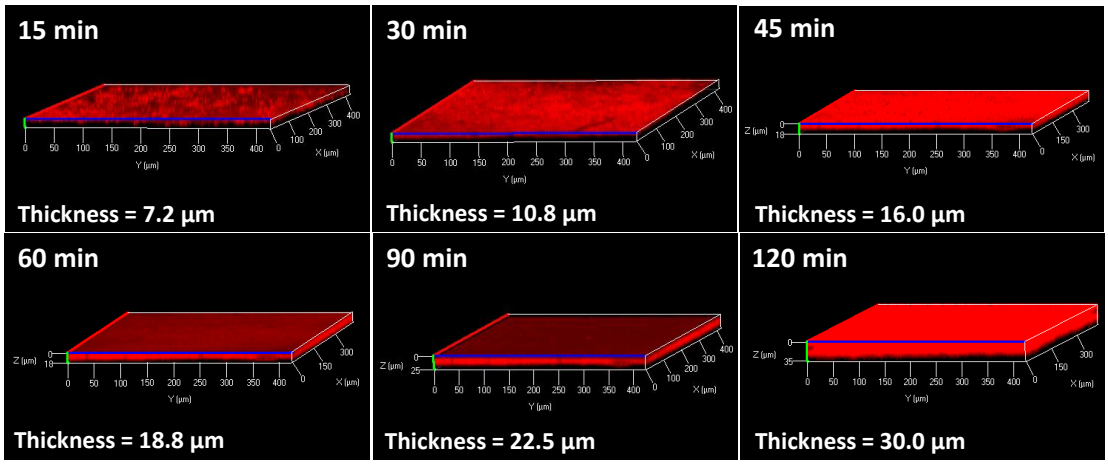

Figure S1. 3D LSCM images of PDA/PSS JMs constructed by varing co-deposition time (from 15 min to 120 min) and thus with different hydrophilization depths (from 7.2 µm to 30.0 µm) wetted by the rhodamine B solution.

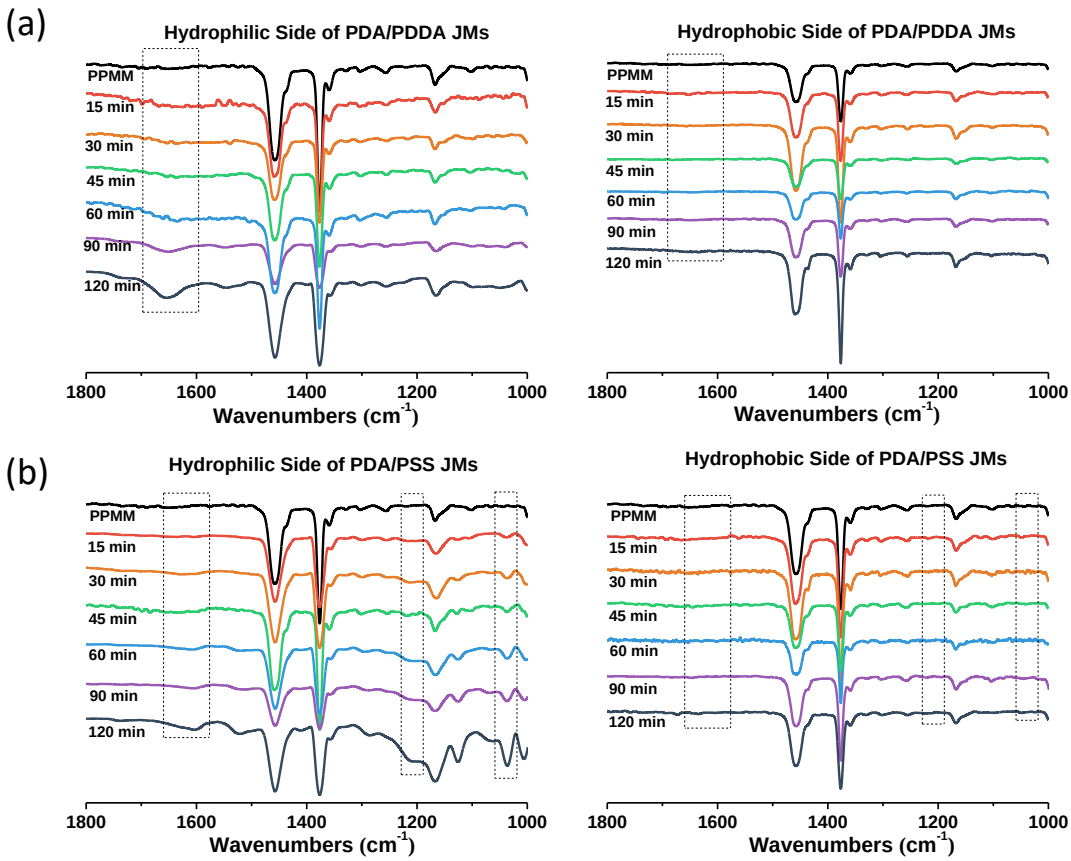

Figure S2. FT-IR/ATR spectra of (a) PDA/PDDA JMs and (b) PDA/PSS JMs for both the hydrophilic side and the hydrophobic side with different co-deposition periods.

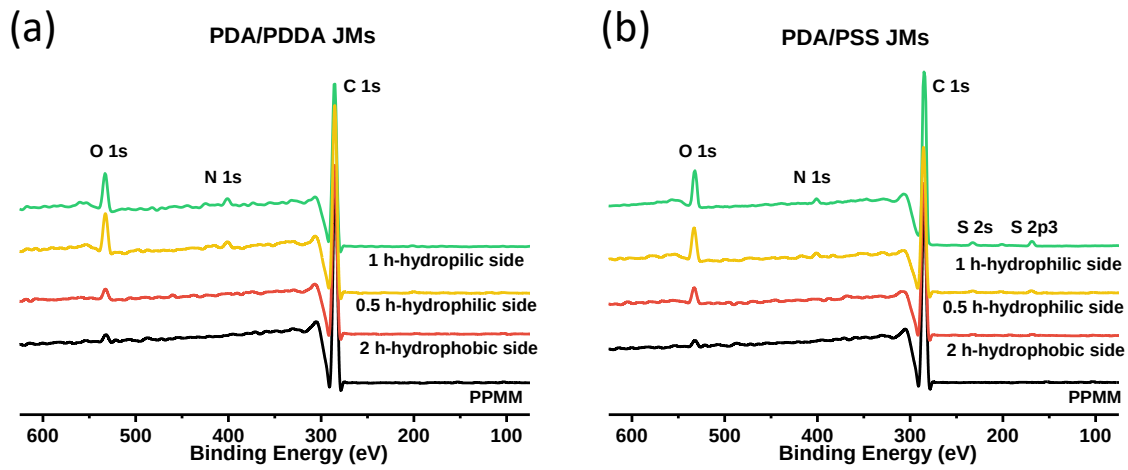

Figure S3. XPS spectra of (a) PDA/PDDA JMs and (b) PDA/PSS JMs for both the hydrophilic side and the hydrophobic side.

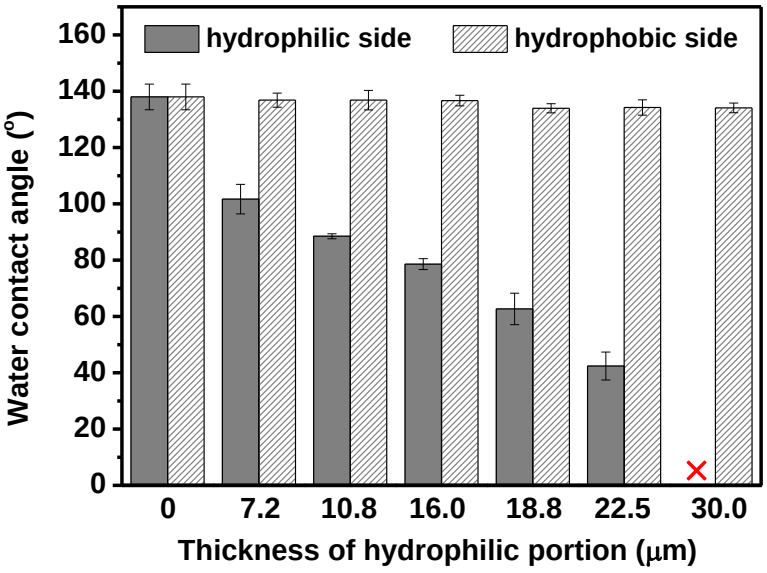

Figure S4. WCA on the hydrophilic side and the hydrophobic side of PDA/PSS JMs with different hydrophilization depths.

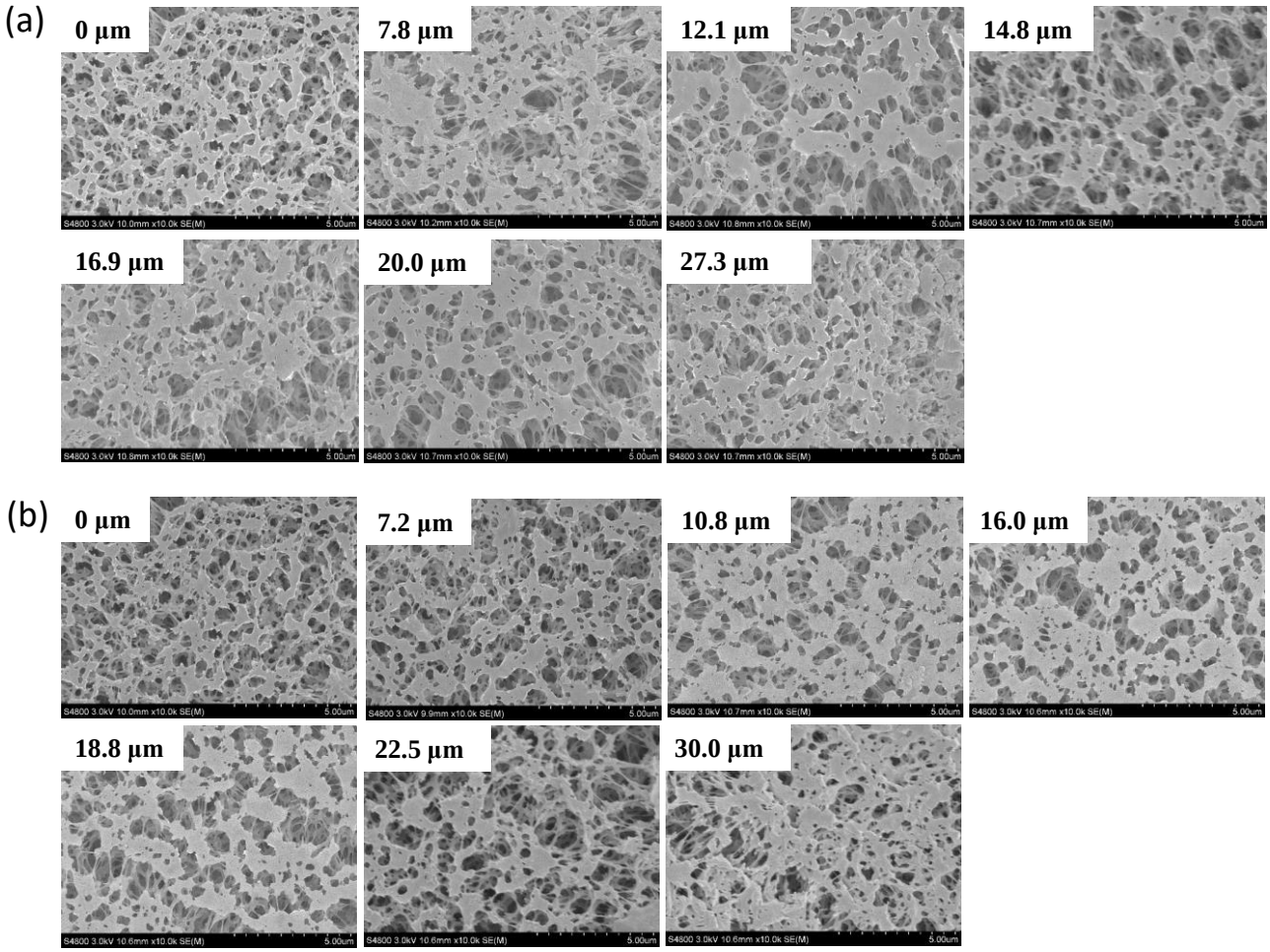

Figure S5. SEM images of the hydrophilic side of (a) PDA/PDDA JMs and (b) PDA/PSS JMs with different hydrophilization depths.

Table S1. Average pore diameter and porosity of nascent PPMM and JMs with different hydrophilization depths.

Samples	Bulk		Surface	
	Average pore diameter (nm)	Porosity (%)	Average pore diameter (nm)	Porosity (%)
Nascent PPMMs	245.4	73.2	190.2	30.7
PDA/PDDA JMs (7.8 μm)	---	---	157.3	28.5
PDA/PDDA JMs (12.1 μm)	262.3	73.2	185.5	37.1
PDA/PDDA JMs (14.3 μm)	276.3	73.4	236.9	39.8
PDA/PDDA JMs (16.9 μm)	---	---	167.5	31.0
PDA/PDDA JMs (20.0 μm)	---	---	178.2	31.1
PDA/PDDA JMs (27.3 μm)	260.0	73.0	147.7	27.4
PDA/PSS JMs (7.2 μm)	---	---	197.4	36.7
PDA/PSS JMs (10.8 μm)	242.0	72.8	174.7	29.9
PDA/PSS JMs (16.0 μm)	250.7	73.1	189.9	36.6
PDA/PSS JMs (18.8 μm)	---	---	208.0	39.2
PDA/PSS JMs (22.5 μm)	---	---	243.9	39.4
PDDA/PSS JMs (30.0 μm)	273.2	73.4	179.9	24.1

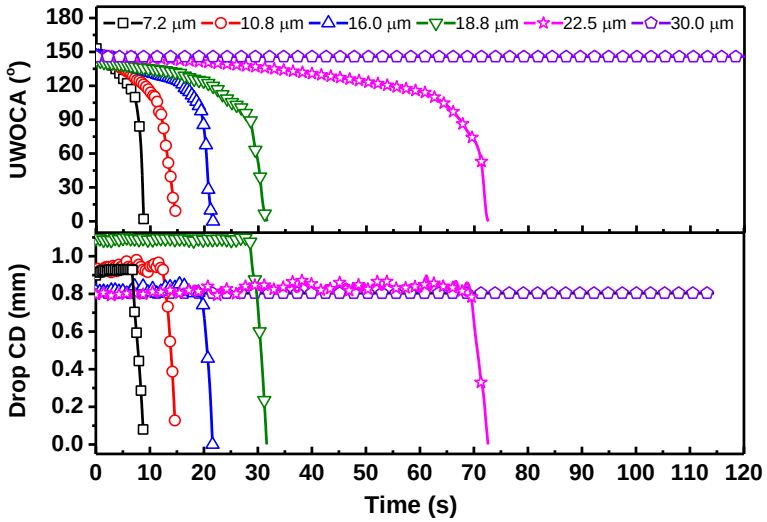

Figure S6. Dynamic UOCA and oil drop CD on the hydrophilic side of PDA/PSS JMs with different hydrophilization depths.

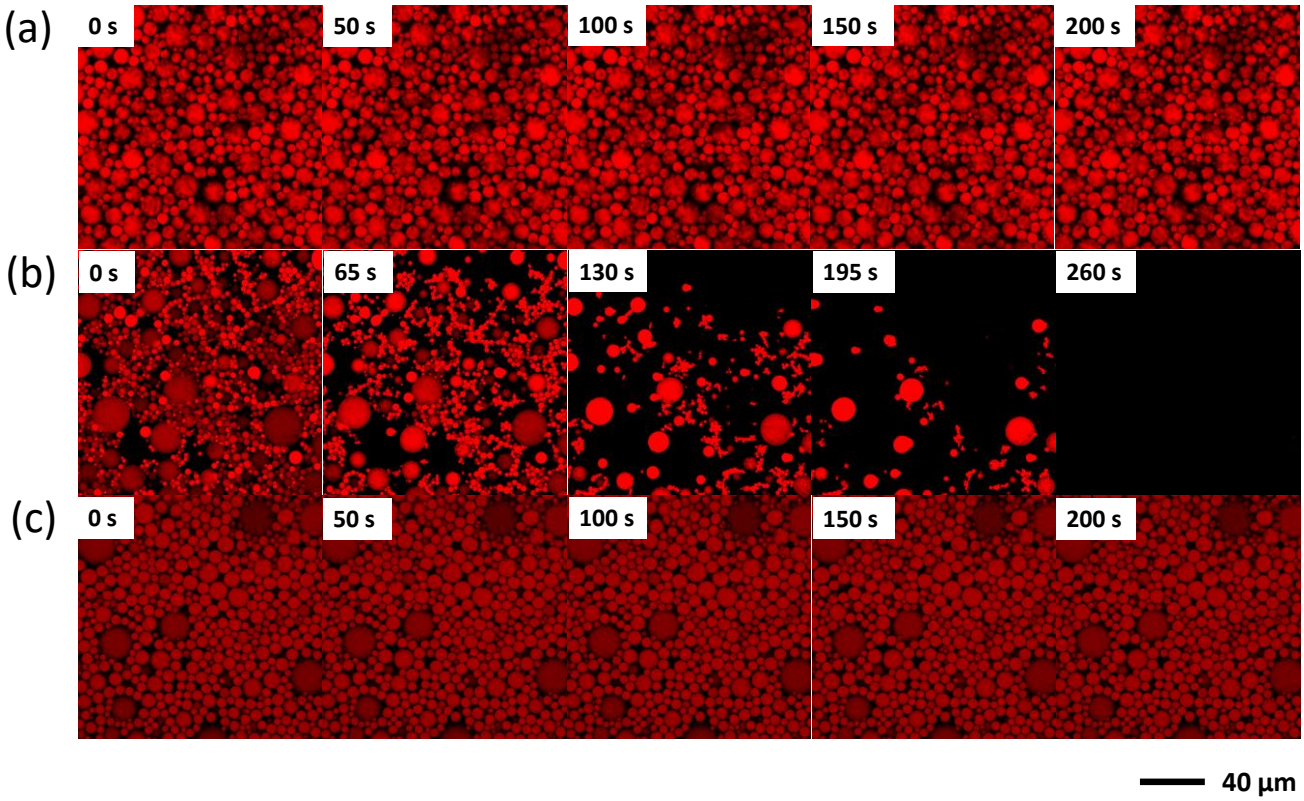

Figure S7. LSCM images of emulsion separation processes using PDA/PSS JMs with different hydrophilization depths: (a) H_1 = 0 μm (neat PPMM), (b) H_1 = 10.8 μm, (c) H_1 = 30.0 μm. The oil-in-water emulsions are stabilized by hexadecyl trimethyl ammonium bromide (CTAB) and dyed by Nile red.

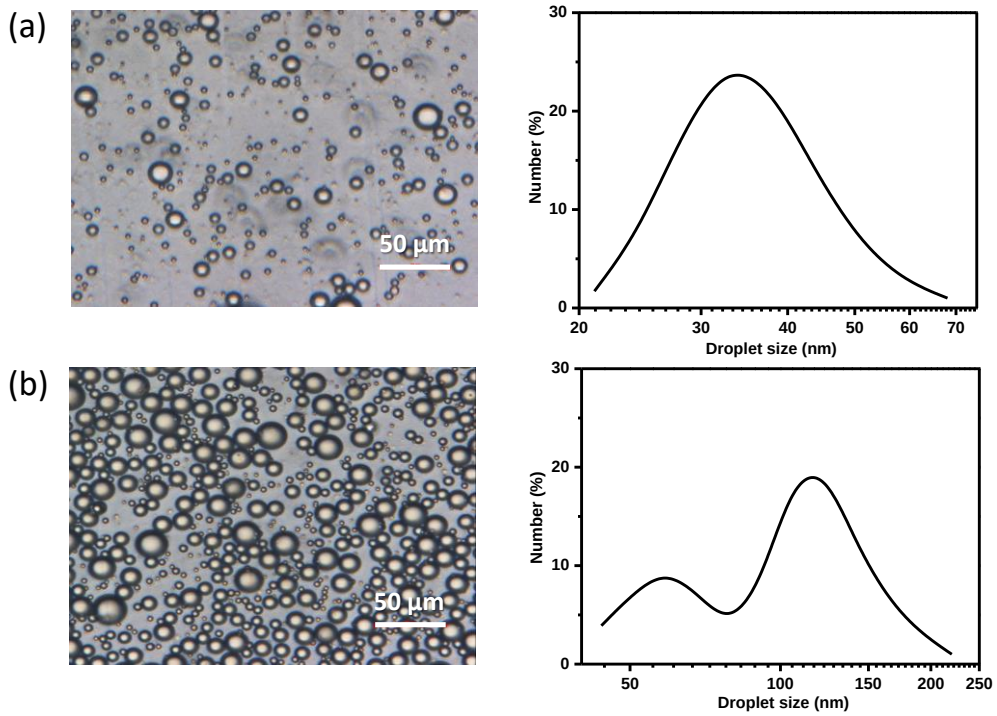

Figure S8. Optical microscopic photos (left) and DLS graph (right) of (a) Tween 80 stabilized and (b) CTAB stabilized emulsions. The oil contents are 100 mg/mL and 15 mg/mL for (a) and (b), respectively.

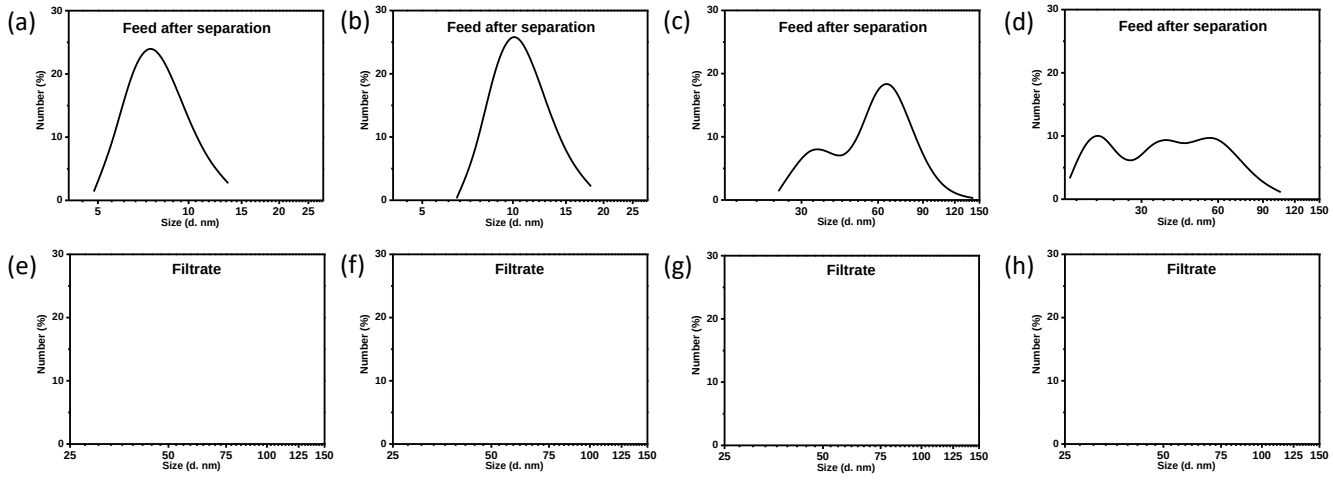

Figure S9. DLS graphs of feed after separation for (a) PDA/PDDA JMs toward SDS stabilized emulsions, (b) PDA/PSS JMs toward CTAB stabilized emulsions, (c) PDA/PDDA JMs toward Tween 80 stabilized emulsions, and d) PDA/PSS JMs toward Tween 80 stabilized emulsions. The corresponding DLS graphs of filtrate after separation for (a), (b), (c) and (d) are shown in (e), (f), (g) and (h).

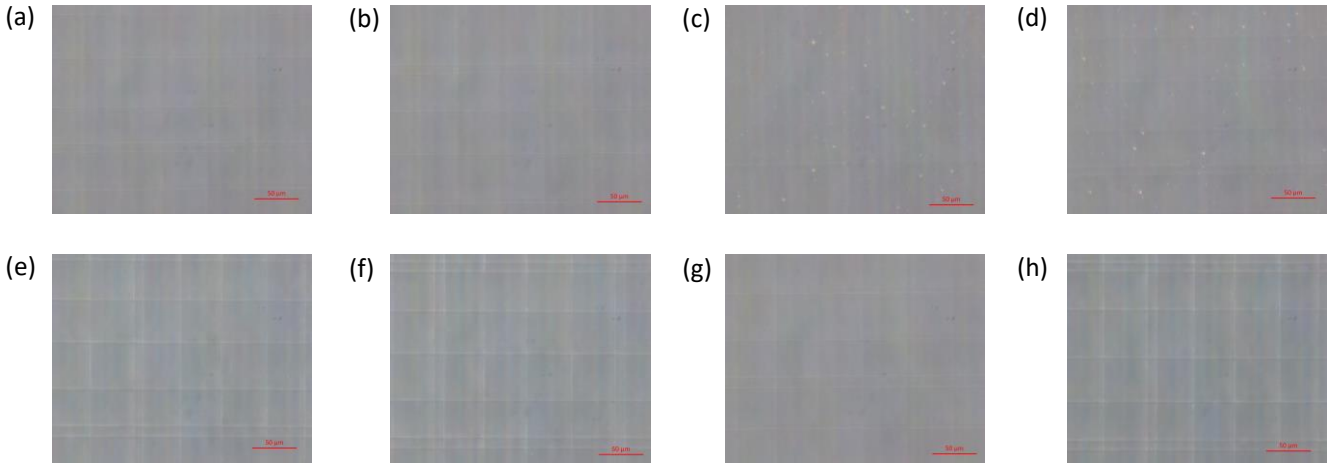

Figure S10. Optical microscopic images of feed after separation for (a) PDA/PDDA JMs toward SDS stabilized emulsions, (b) PDA/PSS JMs toward CTAB stabilized emulsions, (c) PDA/PDDA JMs toward Tween 80 stabilized emulsions, and (d) PDA/PSS JMs toward Tween 80 stabilized emulsions. The corresponding optical microscopic images of filtrate after separation for (a), (b), (c) and (d) are shown in (e), (f), (g) and (h).

Table S2. Purities of collected oils using different Janus membranes after separation.

Sample	Oil purity (%)
PDA/PDDA JM (H_1 = 12.1μm) / SDS emulsion	98.8
PDA/PSS JM (H_1 = 10.8 μm) / CTAB emulsion	99.9
PDA/PDDA JM (H_1 = 12.1 μm) / Tween 80 emulsion	99.6
PDA/PSS JM (H_1 = 10.8 μm) / Tween 80 emulsion	99.5

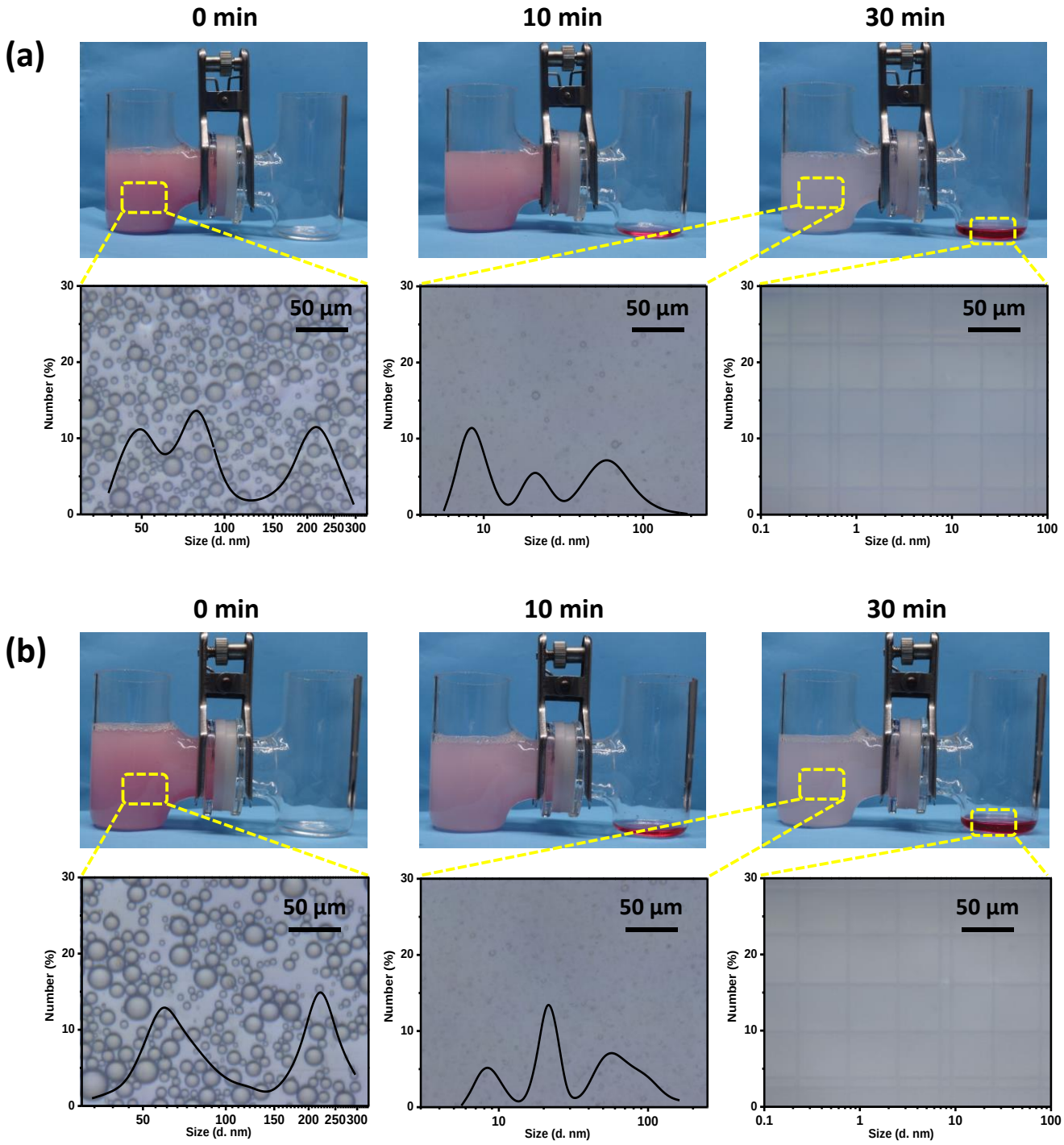

Figure S11. Photographs of petroleum ether separation status at time t=0, 10, 30 min for oil-in-water emulsions stabilized by (a) SDS using PDA/PDDA JMs (H_1 = 12.1 μm) and by (b) CTAB using PDA/PSS JMs (H_1 = 10.8 μm). The optical microscopic images and DLS graphs of feed before and after separation as well as filtrate after separation are shown correspondingly.

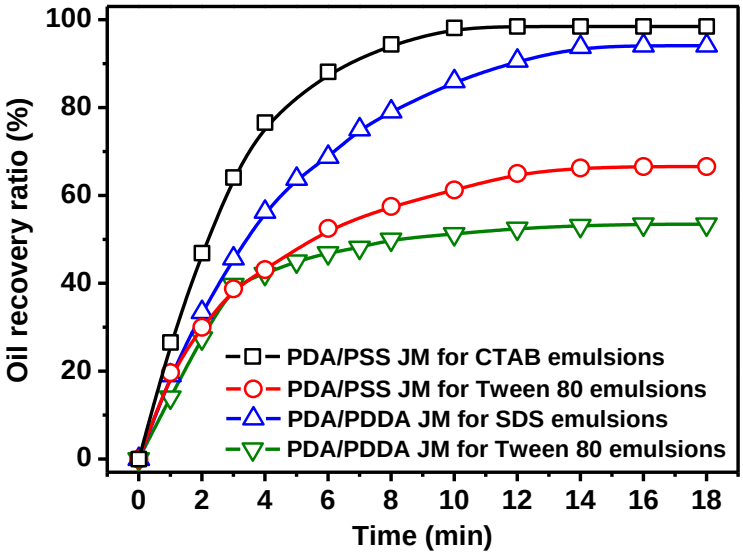

Figure S12. Comparison of separation data for oil-in-water emulsions stabilized by different surfactants using PDA/PDDA or PDA/PSS JMs with ~10 μm of hydrophilization depth.

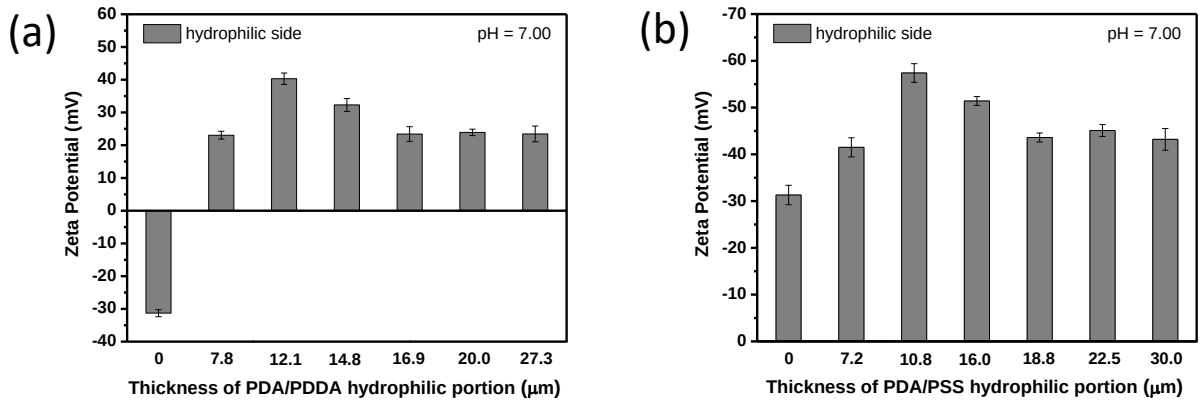

Figure S13. Surface zeta potential of the hydrophilic side as a function of the hydrophilization depth for (a) PDA/PDDA JMs and (b) PDA/PSS JMs.

In the case of coexisted DA and polyelectrolytes in aqueous solution, the oxidative polymerization of DA can produce two kinds of PDA-based colloidal particles. One is neat PDA aggregates containing covalently bonded PDA and physically self-assembled trimers [1]. The other one is charged hybrid PDA/polyelectrolyte clusters formed through electrostatic interactions because PDA owns negatively charged catechol groups as well as positively charged amino groups [2]. Both polycations and polyanions are able to inhibit the growth of PDA aggregates due to the electrostatic stabilization effect [3]. The size of hybrid clusters is thus smaller than that of neat PDA aggregates. Under an electric field, these relatively small and charged hybrid clusters preferentially migrate to the oppositely charged electrode and

adhere onto the membrane surface and inside wall of the pores. However, the deposition of the neat PDA aggregates cannot be accelerated due to their neutral and large-sized profiles. It means that the electric field-accelerating deposition of charged PDA/electrolyte clusters is dominant during the first 30 min until an equilibrium is reached. The deposition of neat PDA aggregates, however, is still in progress afterwards. Such difference in the kinetics of deposition thus causes a maximum value of the surface zeta potential when the membrane was deposited for 30 min (**Figure S13)**. Therefore, those Janus membranes with the most enriched surface charge ($H_1 \approx$ 10 μm) significantly facilitate the deemulsification process, exhibiting excellent separation performances mentioned above. Further, the efficiency of emulsion separation becomes depressed with thickening the hydrophilic depth because the directional oil delivery is hindered gradually.

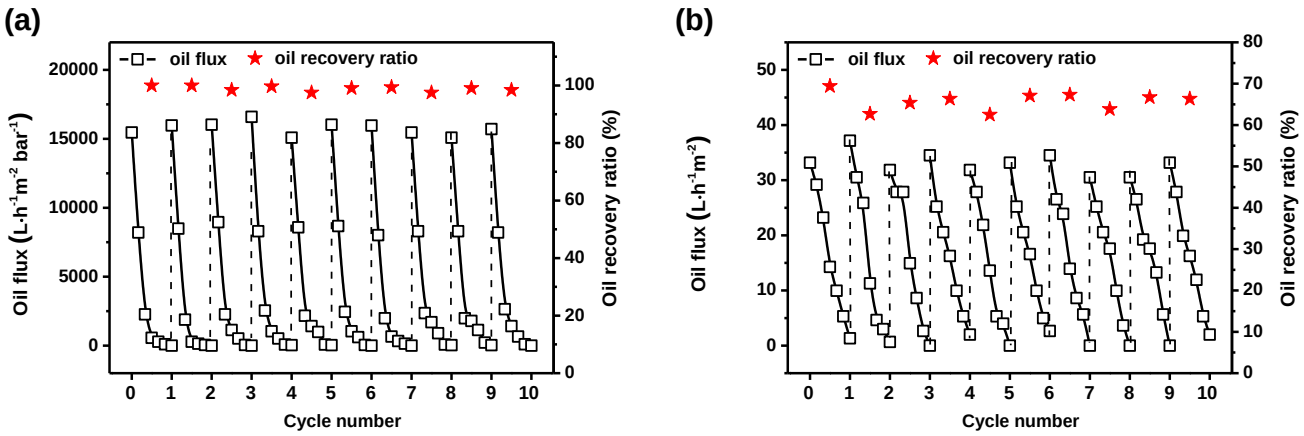

Figure S14. Oil flux and recovery ratio evolutions under repeated cycles when PDA/PSS JMs (H_1 = 10.8 μm) were used to separate the CTAB stabilized oil-in-water emulsions. 1,2-Dichloroethane (a) and petroleum ether (b) were used as the heavy oil and the light oil, respectively.

References

[1] S. Hong, Y. S. Na, S. Choi, I. T. Song, W. Y. Kim, H. Lee, *Adv. Funct. Mater.* **2012**, *22*, 4711-4717.

[2] H.-C. Yang, R. Z. Waldman, M.-B. Wu, J. Hou, L. Chen, S. B. Darling, Z.-K. Xu, *Adv. Funct. Mater.* **2018**, *28*, 1705327.

[3] M. Mateescu, M. H. Metz-Boutigue, P. Bertani, V. Ball, *J. Colloid Interf. Sci.* **2016**, 469, 184-190.